Exploring the Cure State Dependence of Relaxation and the Vitrimer Transition Phenomena of a Disulfide-Based Epoxy Vitrimer

Lorenz, Niklas; Dyer, William E.; Kumru, Baris

DOI
10.1002/pol.20250463

Publication date
2025

Document Version
Final published version

Published in
Journal of Polymer Science

Journal of Polymer Science

WILEY

JOURNAL OF POLYMER SCIENCE

RESEARCH ARTICLE OPEN ACCESS

Exploring the Cure State Dependence of Relaxation and the Vitrimer Transition Phenomena of a Disulfide-Based Epoxy Vitrimer

Niklas Lorenz | William E. Dyer | Baris Kumru

Aerospace Structures & Materials Department, Faculty of Aerospace Engineering, Delft University of Technology, Delft, the Netherlands

Correspondence: Niklas Lorenz (n.lorenz@tudelft.nl)

Received: 22 April 2025 | **Revised:** 5 June 2025 | **Accepted:** 12 June 2025

Funding: This work was supported by the National Growth Fund program NXTGEN HIGHTECH 01 (NGFNH2201).

Keywords: characterization | cure-state dependence | disulfide | epoxy | vitrimer | vitrimer transition temperature

ABSTRACT

Vitrimers are a class of polymer networks featuring dynamic covalent crosslinks that can undergo associative bond exchange. These dynamic polymer networks hold a notable promise as recyclable thermosets with self-healing capabilities, provided by network rearrangements at the molecular level, allowing for macroscopic flow. When the relaxation time is sufficiently short, vitrimer material behaves like a thermoplastic even though it is covalently crosslinked. However, temperature-induced malleability remains limited by the high-viscous nature of vitrimers. Therefore, the present article explores the cure dependence of structural relaxation and vitrimer transition phenomena of a dynamic disulfide-containing epoxy vitrimer. Stress relaxation measurements reveal that intermediate cure states—accompanied by lower crosslinking density—exhibit bond exchange and segmental relaxation rates exceeding those of fully cured networks over an order of magnitude. This enhanced dynamics facilitates lower viscosities and residual times during high-temperature malleability processing. Advanced methods combining rheology, cure kinetics, and thermomechanical analysis are utilized to assess the cure dependence of the vitrimer transition temperature T_v. We outline a distinct cure dependence of T_v, which may be approximated by a linear correlation, suggesting that viscoelastic flow can be initiated at significantly lower temperatures in undercured networks. These findings provide valuable guidance for enhancing material and processes, contributing to opening doors to the "melt processing" of this family of materials.

1 | Introduction

Incorporating dynamic covalent bonds into native thermosets enables direct recycling and imparts thermoplastic-like properties such as malleability and self-healing [1, 2]. These dynamic networks, enabled by different chemistries such as transesterification [3], disulfide [4–9], imine [10–12], siloxane [13, 14], and urethane [15] exchange, offer a sustainable alternative to conventional epoxy resins [16, 17].

Before harnessing these advantages, the initial reactive mixtures undergo reactive processing, resulting in full or partial curing. The curing process can be recognized either as a source of variability that increases uncertainty or as a functional attribute facilitating novel material-inherent functions, such as joining [18] and (re)forming features [19]. Undercured resins exhibit unwanted effects such as increased stiffness [20–22] and (depending on the underlying hardener moiety) are prone to brittle cracking [23], which may have detrimental consequences during use. Errors may encompass defects such as part distortion and matrix cracking within the manufactured part [24]. Incomplete curing is accompanied by reduced thermal stability (by decreasing the glass transition temperature T_g). Therefore, ensuring complete cure during processing is desirable, as only

cured materials exhibit high rigidity and high impact resistance [25]. This issue is undoubtedly relevant for resins entering vitrification, confining the reaction process by the glassy state diffusion dynamics and limiting the final degree of cure.

Besides these additional variabilities, incomplete curing and residual soluble fractions can introduce additional plasticizing effects through dangling chains [26]. Consequently, partly cured states may open up novel processing routes such as joining [18] and (re)forming features [19] by deliberately utilizing plasticizing effects that render the materials partially malleable. This effect has not yet been studied in the context of vitrimers but could offer significant advantages in enhancing their malleability. Indeed, the malleability of vitrimers is quite distinct from that of thermosets with permanent crosslinks. When the relaxation time is sufficiently short, vitrimer material behaves like a thermoplastic even though it is covalently crosslinked, enhancing its processability. A controversial but well-established parameter is the vitrimer transition temperature T_v (or topology freezing temperature), which determines the transition from the viscoelastic solid to the viscoelastic liquid (or "melt") state [27]. While the nature of the respective transition phenomenon is still a subject of ongoing scientific debate, different descriptive methods (thermomechanical analysis [28, 29], temperature-dependent tensile creep experiments [3, 30], and different rheological criteria [31, 32]) have been designed to detect the onset of plastic flow, which may be associated with the presence of dynamic covalent bond exchange reactions.

Despite the bond exchange and the resulting macroscopic flow, the highly viscous nature of crosslinked vitrimer matrix materials poses significant challenges in the processing of thermosets by preventing (inter) layer sliding [33] and wrinkling of fibers [34], thus limiting the processability. Even though the extrusion of vitrimers has been demonstrated in literature [35, 36], "melt" processing appears to be reserved for specially tailored material formulations with artificially accelerated bond exchange reaction rates rather than the broad majority of reported vitrimer systems. Besides that, some authors describe the preparation of "pre-vitrimers" [37, 38], which can be processed in the "melt" stage (e.g., hot melt adhesive, extrusion, and injection molding) before gelation. Subsequent heating initiates the final crosslinking. However, the percolated state and its relaxation and initiation of plastic flow are not specifically investigated.

In this context, it seems necessary to increase bond exchange reaction rates (and decrease accompanying viscosity) to bridge the gap between the high-viscous flow characteristics of vitrimers and the viscosities required for processing in established polymer manufacturing processes, such as thermoforming, extrusion, or even injection molding. Therefore, several strategies are available to accelerate the bond exchange reactions of disulfides, allowing precise control over relaxation times and viscosities. Since these dynamic covalent moieties are embedded within a network, their exchange capacity is inherently affected by the mobility of the surrounding network [4, 39]. Azcune et al. investigated the effect of crosslinking density and disulfide concentration on the bond exchange dynamics. Reducing the crosslinking density improves the bond exchange reaction rates, presumably due to lower viscosity, while increased disulfide concentrations yield significantly faster relaxation times in the low-temperature regime [5]. Furthermore, the presence of free pending amine groups accelerates the exchange kinetics [6, 40] and may be used to tailor the dynamic properties.

Investigating how the plasticizing effect in partially crosslinked networks accelerates bond exchange and segmental relaxation is crucial for enhancing the processability of vitrimers. Specifically, plasticizing effects in partially crosslinked networks could contribute to accelerating bond exchange and segmental relaxation, ultimately reducing viscosity and improving processability. Moreover, disulfide-containing aromatic amine compounds may possess dynamic bonds under mild conditions [41] or ambient temperature [42] (even if chain mobility remains confined in the glassy state), so the dynamic bond exchange should remain permissible for partly cured systems even at mild temperatures—at the same time minimizing the effects of enhancing curing reaction.

To the best of our knowledge, the relationship between cure state, segmental relaxation, bond exchange kinetics, and the T_v in percolated networks remains unexplored. Our experimental research addresses this critical gap by systematically elucidating how varying cure states influence these essential vitrimer characteristics. First, reaction kinetics are derived (Section 3.1) to estimate cure advancement during elevated temperature testing and tailor cure cycles for manufacturing samples with different cure states (Section 3.2). Based on that, the cure-state dependence of thermomechanical properties (Section 3.3), segmental relaxation and bond exchange dynamics (Section 3.4), and T_v (Section 3.5) are investigated. Finally, we compile all data into a conversion–temperature phase diagram (Section 3.6), which incorporates the cure dependence of T_v. We indicate generic processing cycles that intentionally leverage the cure-state dependence of the dynamic network to exploit the enhanced malleability in the partially crosslinked state.

2 | Materials and Methods

2.1 | Materials

1,4-Butanediol diglycidyl ether (BDE, epoxy equivalent weight of 101.125 g/eq.) and 4-aminophenyl disulfide (4-AFD, amine equivalent weight of 62.093 g/eq.) are purchased from Sigma-Aldrich Corp., Netherlands, and Molekula Ltd., UK, respectively. Small batches of reactive mixtures are prepared according to the procedure described in the Supporting information while maintaining the epoxide: amine ratio at the stoichiometric balance of 2:1.

2.2 | Characterization

Differential scanning calorimetry (DSC, mDSC250 device from TA Instruments Inc.) is applied to analyze the curing process based on the exothermal heat flow released during epoxy-amine curing. Dynamic DSC scans with 2, 4, and 8 K min^{-1} are carried out at temperatures ranging from −90°C to 250°C to determine the initial glass transition temperature $T_{g,0}$ of the uncured mixture and capture the heat flow during the curing reaction. Furthermore, isothermal dwellings at 110°C, 130°C, and 150°C

are selected to characterize the kinetics of the isothermal curing process. The final glass transition temperature $T_{g,\infty}$ is determined after submitting the resin to an isothermal dwelling at 150°C for 3 h before cooling to 25°C. Subsequent reheating at 5 K/min determines $T_{g,\infty}$ of the samples.

For the thermomechanical and mechanical analysis described in the following, neat resin specimens of different geometries were manufactured according to the methods described in the Supporting information. Dynamic mechanical analysis (DMA, RSA-G2 device from TA Instruments, USA.) pursues two objectives: characterizing the temperature-dependent module development for different cure states (i) and characterizing the bond exchange kinetics of the disulfide bonds employing stress relaxation tests in the rubbery regime (ii). All DMA testing was performed utilizing a film tensile clamp. For (i), rectangular specimens ($6\times0.8\times30\,mm^3$) were heated under air with a rate of $3\,K\,min^{-1}$ from −50°C to 150°C with a static tensile force of 0.01 N and a frequency of 1 Hz while applying a dynamic displacement of 0.1% (in the linear viscoelastic region). For (ii), the fully cured material was exposed to isothermal stress relaxation trials under air using instantaneous stress of 2% within 0.1 s at temperatures ranging from 140°C to 240°C. Furthermore, relaxation tests were carried out at 140°C to analyze the cure-state dependence of the dynamic bond exchange. The temperature selected is explicitly low, so only a marginal progression of the curing reaction is expected during the 2-min soaking and subsequent relaxation times.

Thermomechanical analysis (TMA, TMA 4000 from PerkinElmer Corp., USA.) was utilized to capture the initiation of flow and associated T_v, applying the technique proposed by Hubbard et al. [29]. Heating rates of $5\,K\,min^{-1}$ were used, and a nominal force of 0.1 N maintained the contact of cylindrical specimens (with a diameter of 4 mm and a thickness of 1.8 ± 0.05 mm) and the glass probe (4 mm diameter) during the measurement. Since T_v is significantly affected by the heating rate and the applied stress [29, 30]; we employ constant parameters during all measurements. The top and bottom sample surfaces of the specimens molded in the metal tool are smooth and plain, so no additional surface finishing was required. Before testing, thin aluminum foils are placed on the bottom and top surface of the resin specimen to prevent adhering sticky samples to the testing device and reduce friction in the radial direction [29]. The thermal expansion of the aluminum film does not significantly contribute to the measured overall thermal expansion (Figure S7), and the accompanying absolute error in the measured total strain is located below 0.5%. Furthermore, the samples are mounted at temperatures above the glass transition temperature to relax frozen residual stresses (and eliminate any metastable material states imposed by the manufacturing process [28]) within the glassy material state and avoid an excessive penetration of the specimen by the probe during the glass transition. After mounting the specimen and applying the nominal force, the specimens are cooled to −50°C and then reheated to 200°C in a nitrogen atmosphere.

Rheometry (HAAKE MARS III, Thermo Fisher Scientific Inc., USA) is utilized to determine the gelation point (GP) and to measure the chemical shrinkage according to the methodology proposed by Haider et al. [43] to derive a phenomenological model that describes cure-dependent chemical strains. For measuring the GP, isothermal oscillating measurements at 1 Hz are conducted at temperatures ranging from 120°C to 150°C with a deformation amplitude of 0.1% in the parallel plate configuration (diameter 20 mm) and a gap of 1 mm. A temperature-controlled test chamber realized heating with temperature tolerances set to 0.1°C. Previous strain sweeps ensure the applied strain was within the linear viscoelastic region of the polymer.

3 | Results and Discussion

First, the curing kinetics are examined, providing the foundation for designing cure cycles applied to manufacture specimens with well-defined varying cure states for further testing (Section 3.2). Subsequently, the effect of the cure state on the thermomechanical material response (Section 3.3), the segmental relaxation and bond exchange kinetics (Section 3.4), and the initiation of macroscopic flow represented by T_v (Section 3.5) are discussed. Finally, we compile all data into CTP diagrams and discuss practical implications.

3.1 | Reactions Kinetics Modeling

The heat flow signals are integrated to calculate reaction enthalpy using a linear baseline for dynamic and a strictly horizontal baseline for the isothermal runs. We assume that the enthalpy measured corresponds only to the epoxy-amine curing, as any energy exchange due to disulfide bond exchange exhibits a zero net effect. A total reaction enthalpy $\Delta H_{R,total}$ value of $553\pm12\,J\,g^{-1}$ is located in the range of vitrimers utilizing the same disulfide curing agent [9, 44].

Three isothermal (110°C, 130°C, and 150°C) and three dynamic (1, 2, and $4\,K\,min^{-1}$) scans were evaluated simultaneously using multivariate analysis to account for isothermal and nonisothermal conditions during curing. Encompassing isothermal besides the nonisothermal measurements in the fitting routine ensures accurate modeling of isothermal cure [45]. The phenomenological Kamal Sourour approach provides the basis for the proposed modeling approach [46, 47]. Combining an *n*th order and an autocatalytic model represents an established approach for the curing behavior of epoxy resins and the development of the degree of cure ξ [46, 48–50]:

$$\frac{d\xi}{dt} = \left(k_1 + k_2\xi^m\right)(1-\xi)^n \tag{1}$$

As the developing T_g is unlikely to exceed the isothermal curing temperature, the reactions are maintained in the kinetically controlled regime, and the chemical kinetic constants $k_{i,chem}$ exhibit Arrhenius-like behavior:

$$k_i = A_i e^{-E_i/RT} \tag{2}$$

The differential equation (Equation 1) is solved numerically with the initial condition $\xi = 0$, and the six independent model parameters $(E_1, E_2, A_1, A_2, m, n)$ are estimated simultaneously for three isothermal and three nonisothermal datasets utilizing a generic algorithm.

TABLE 1 | Parameters for the reaction kinetic modeling disrobed by Equations (1,2).

$A_1\left[\log\left(s^{-1}\right)\right]$	$E_1\left[kJ\ mol^{-1}\right]$	$A_2\left[\log\left(s^{-1}\right)\right]$	$E_2\left[kJ\ mol^{-1}\right]$	m	n
4.91	68.37	4.79	59.02	0.91	1.54

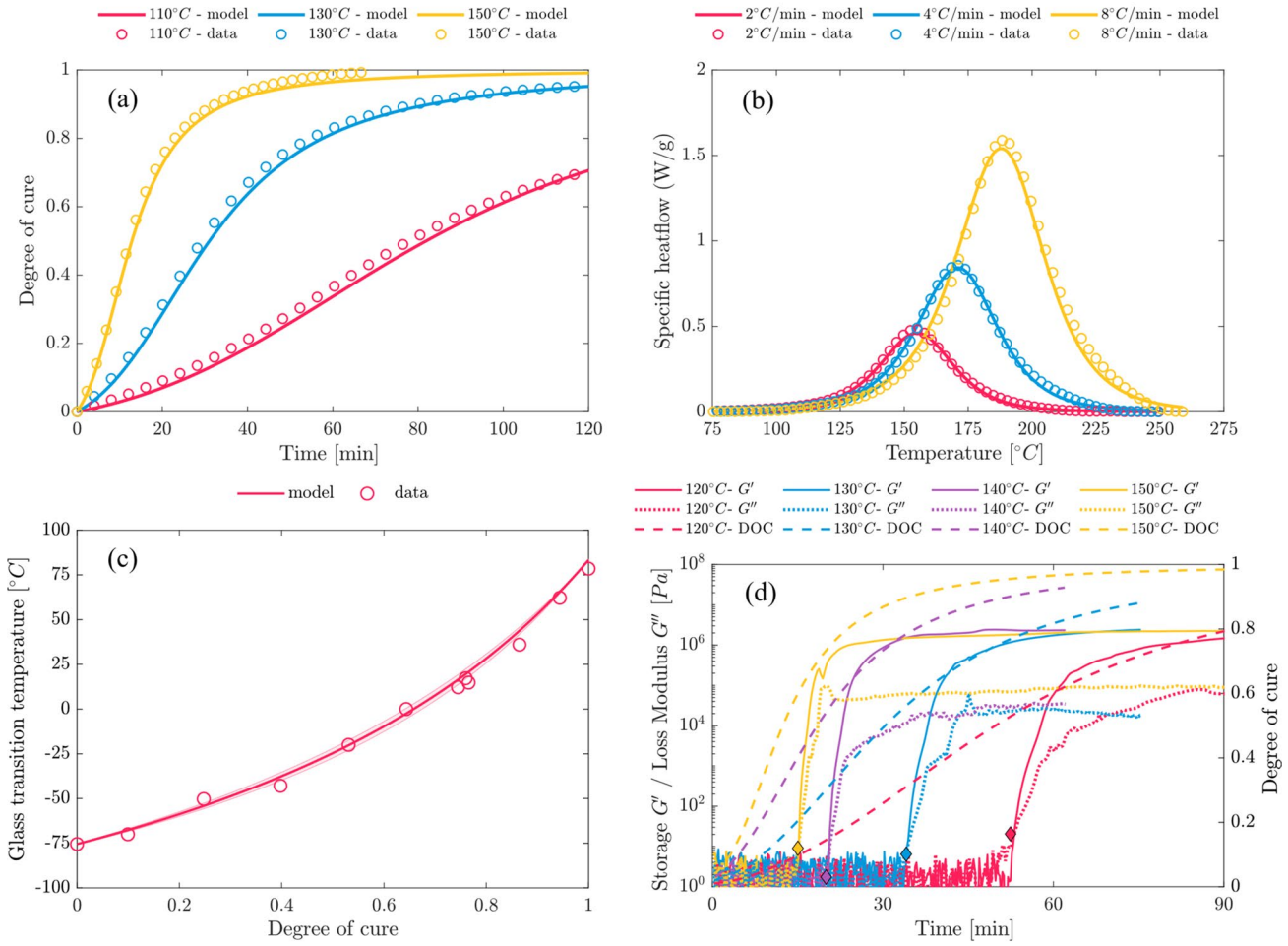

FIGURE 1 | Comparison of data and model for isothermal (a) and nonisothermal (b) curing conditions. For (b), the heat flow of the model is calculated by assuming the generally accepted direct proportional relation of $d\xi\,/\,dt$ and apparent exothermal heat flow with the total reaction enthalpy $\Delta H_{R,total}$ being the proportional factor. Cure dependence of glass transition temperature approximated by Di-Benedetto equation (c). Isothermal oscillating dwellings at different temperatures are used to measure gelation and calculate the degree of cure (DOC) (d). The intersection of G' and G'' is marked with a diamond.

Table 1 summarizes the model parameters, and Figure 1a,b compares measurement data and model. A mean average error of 1.1% indicates an excellent agreement between the measurement data and the model.

Besides, it is essential to consider the cure-dependent development of the glass transition temperature $T_g(\xi)$, as with enhancing $T_g(\xi)$, the curing reaction may come to an end for $T_g(\xi) - T < 20 - 30\,°C$ for practical purposes [51]. For our case, we can make selective use of this context to define a temperature window for testing (without significant post-curing) and select appropriate temperatures to prevent full curing or vitrify partially crosslinked states. Therefore, $T_g(\xi)$ is approximated by the Di-Benedetto equation [52]:

$$\frac{T_g - T_{g,o}}{T_{g,\infty} - T_{g,0}} = \frac{\lambda\xi}{1-(1-\lambda)\xi},\quad 0<\lambda<1 \tag{3}$$

with $T_{g,0}$ representing the initial, $T_{g,\infty}$ the final glass transition temperature, and λ, a fitting parameter. Figure 1c shows the glass transition temperature development during curing, and Table 2 summarizes the corresponding parameters. Typically, T_g increases during curing, at the same time yielding a higher crosslink density [53]. For the investigated formulations, glass transition temperature rises from initial values of −75.5°C to 82.3°C. The parameter λ calculates from the quotient $\lambda = \Delta c_{p,\infty}\,/\,\Delta c_{p,0}$ of the specific heat capacity change in the fully cured $\Delta c_{p,\infty}$ and initial state $\Delta c_{p,0}$ [51]. Therefore,

TABLE 2 | Parameters according to Equation (3).

$\Delta c_{p,\infty}$	$\Delta c_{p,0}$	λ	$T_{g,0}$[°C]	$T_{g,\infty}$ [°C]
0.67 ± 0.03	0.32 ± 0.02	0.47 ± 0.04	−75.5 ± 0.22	81.4 ± 0.14

modulated DSC measurements (1 K for 60 s) at 3 K/min are conducted from −90°C to 200°C to determine $\Delta c_{p,0}$ and $\Delta c_{p,\infty}$. Unfortunately, these values show a fair amount of scatter (c.f. Table 2). Therefore, to additionally confirm the correlation's validity, specimens were exposed to isothermal dwellings for specific times and rapidly cooled by 80 K/min to −90°C to derive partly cured states. Subsequent, reheating to 200°C at 3 K min^{-1} allows us to determine pairs of $T_{g,i}$ and ξ_i with ξ_i being calculated from the residual reaction enthalpy $\Delta H_{R,i}$ according to Equation (4) [54]:

$$\xi_i = 1 - \frac{\Delta H_{R,i}}{\Delta H_{R,total}} \tag{4}$$

whereas $\Delta H_{R,total}$ represents the averaged total reaction enthalpy of all nonisothermal DSC. As can be seen from Figure 1c, all the measured values are located within the error tolerance of λ, so that the mean of λ is applied within the present study. Furthermore, a slight discrepancy is found between the midpoint $T_{g,\infty}$ measured by DSC (78°C ± 1°C) and DMA evaluating tan δ peak (82°C ± 1°C). To avoid numerical values without physical meaning (e.g., $\xi > 1$, $T_g > T_{g,\infty}$), $T_{g,\infty}$ is set to 82.3°C.

The network needs to transition into the percolated state (above a degree of cure threshold ξ_{GP} at which the incipient percolated network forms) to ensure that the partly cured samples can be adequately handled in the rubbery state. Within the present work, utilize the crossover of G' and G'' at 1 Hz as a rheological criterion to define the GP as suggested in [55]. Indeed, the rheology-based Winter-Chambon criterion [56] is well established for determining the GP of thermosets but ensuring the selected isothermal curing temperatures exceed the glass transition temperatures at GP ($T > T_{g,GP} + 30^{\circ}C$) as proposed in [55], the G' and G'' criterion remains valid. Typically, gelation is characterized by a temperature-independent degree of cure at gelation ξ_{GP} rather than a (temperature-dependent) specific time [57]. Combining isothermal oscillating rheometer measurements with the reaction kinetics enables us to calculate ξ_{GP} solving Equations (1,2) for the temperature profile recorded during the isothermal dwellings (Figure 1d). An initial degree of cure of 0.01 compensates for the 30 s that elapse between filling and closing the rheometer gap and starting the measurement. The calculations yield ξ_{GP}=0.56 ± 0.03, which is in good agreement with the theoretical value of 0.58 calculated according to the Flory-Stockmayer equation (Table S1). Divergences may be explained by the standard error of the kinetic model and temperature differences between the recorded and the actual temperature present within the resin specimen. With the reaction kinetics now thoroughly characterized, we establish a foundation for manufacturing specimens with specific cure states and examine their properties (Tables 2 and 3).

TABLE 3 | Details on five different cure-states.

	$T_{g,DSC}$ [°C]	ξ_{DSC} [−]	$T_{g,DMA}$ [°C]
$T_{g,1}$	10.7	0.74	10.4 ± 0.7
$T_{g,2}$	21.2	0.79	20.4 ± 0.4
$T_{g,3}$	41.9	0.88	48.5 ± 0.5
$T_{g,4}$	61.6	0.95	67.4 ± 0.1
$T_{g,5}$	78.7	1.00	81.4 ± 0.1

3.2 | Design of Cure Cycles to Manufacture Specimens With Different Cure States

Customized curing cycles are derived to manufacture test specimens with pre-defined cure states based on previous investigations into the fundamental analysis of the curing behavior. The aim is to include the cure dependency ranging from 1 to 0.58 with the lower limit set by percolation. Indeed, one must consider that exothermic overheating and deviation boundary conditions may cause significant deviations from the predicted cure state [58–60], and temperature variations dominate uncertainties, yielding differences in apparent and predicted degrees of cure [61]. Even for specimens of 2 mm thickness, Müller-Pabel demonstrates excessive T_g increase of up to 5 K [62]. Therefore, the curing time is initially estimated conservatively, and the resulting T_g and degree of cure values are confirmed using DSC. The curing process is thus adjusted iteratively to tailor the resulting glass transition temperature (Table 3) reproducibly to defined values, even for varying sample thicknesses (which is of subordinate importance in our case). Although the total reaction heat is considerable, the heat flow remains minimal due to the slow reactivity at the projected initial curing times of 110°C. Unfortunately, smaller values than $T_g = 10.7$ ($\xi = 0.74$) could not be achieved, as it did not seem practicable to accurately handle and analyze test specimens due to low stiffness and intrinsic stickiness.

The detailed manufacturing process, including selected cure cycles, is reported in Table S2 in the Supporting information.

3.3 | Dynamic Thermomechanical Analysis

The cure dependence of the thermomechanical behavior is assessed using small oscillation temperature ramps in the tensile mode. The test specimens in a partly crosslinked state are carefully mounted to the clamps (cf. Section S4). Figure 2a shows the temperature-dependent modulus for different cure states denoted $T_{g,1}$–$T_{g,5}$. The glass transition temperatures of the partly cured states determined according to the tan δ peak criterion are shown in Table 3. With decreasing cure-state, the width of the

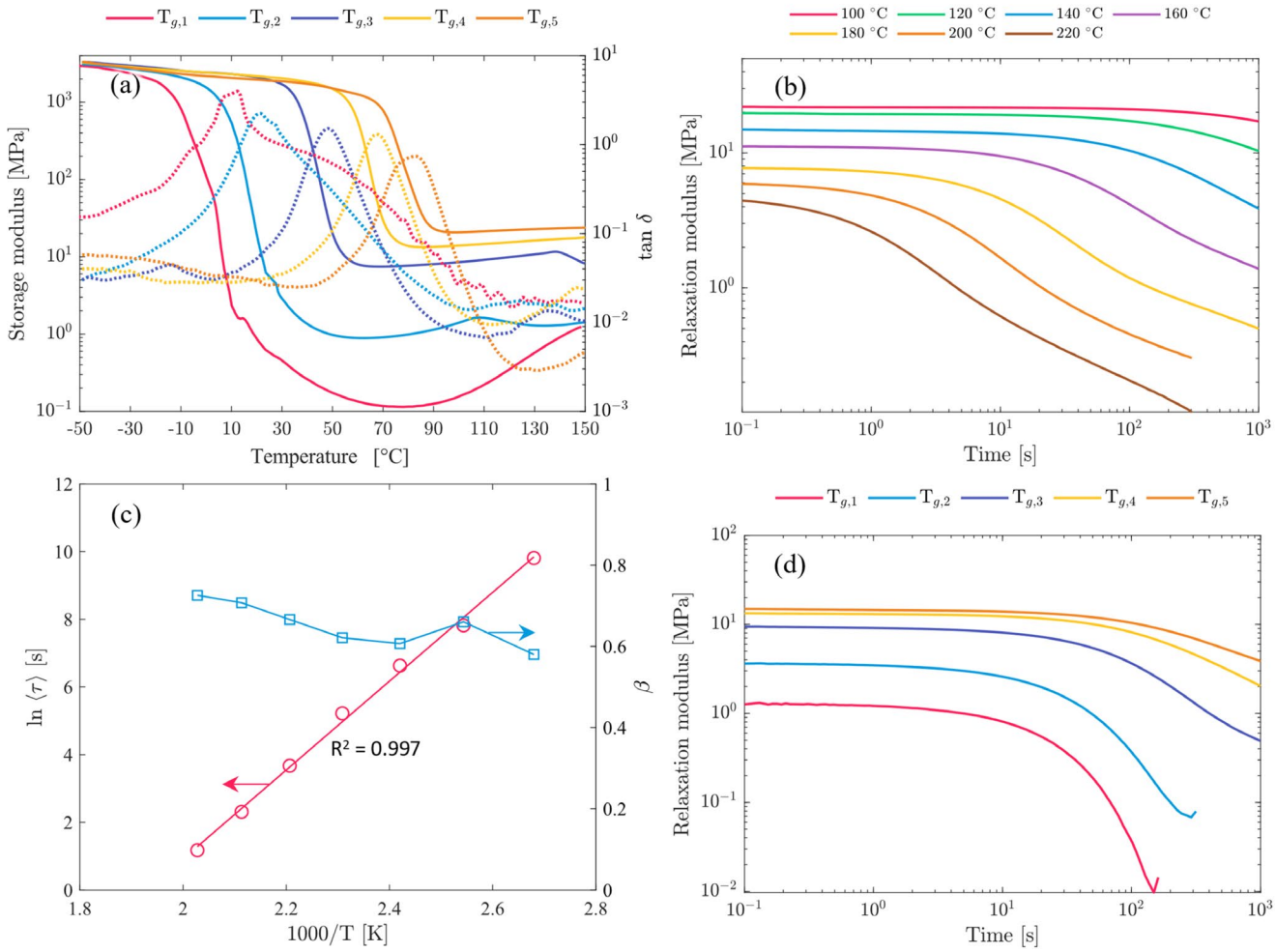

FIGURE 2 | Module development for the different cure states $T_{g,1}$–$T_{g,5}$ (a). Tensile stress relaxation experiments for the fully cured material $T_{g,5}$ for temperatures ranging from 100°C to 220°C (b). Stretching exponent β and average relaxation times $\langle\tau\rangle$ according to Kohlrausch–Williams–Watts function (c). Tensile stress relaxation experiments for different cure states $T_{g,1}$–$T_{g,5}$ (d).

tan δ peak width increases, indicating a more inhomogeneous network structure [63]. The partly cured states reduce the number of crosslinking points so that the T_g decreases. Furthermore, the intensity of tan δ peaks directly relates to the extent of motion associated with the glass transition. Consequently, the more flexible structure of the partly cured system—confirmed by the presence of soluble fractions (cf. Figure S2) increasing the segmental mobility by plasticizing effects—maintains its mobility (significantly lower $E^{'}$, Figure 2a), manifesting in a greater reduction in tan δ peak intensity.

While the higher storage moduli confirm the expected slight increase in stiffness [20, 23] for cure states $T_{g,1}$–$T_{g,3}$ (cf. Table S3) an inverse correlation is observed for $T_{g,4}$ and $T_{g,5}$ as temperatures of −50°C already initiate the α-relaxation, involving the local motion of flexible long-chain aliphatic groups (and therefore decreasing the modulus) that trigger the many molecule cooperative glass transition.

Indeed, an advancing cure cannot be excluded during testing and is calculated based on the recorded temperatures and Equations (1,2). The results are provided in Table S4 and Figure S1, stating an increase of up to 0.1. It becomes apparent that the exclusive increase in rubbery modulus of the partly cured specimens starting at temperatures of 90°C–105°C matches the initiation of the (post) curing process during the DMA measurements (cf. Figure S1). One may attribute the steady increase in rubbery modulus to the advancing curing reaction.

Besides that, with a decreasing cure state, the rubbery modulus $E'_{T_g+50°C}$ significantly decreases by up to two magnitudes. Still, especially for the partly cured states, we are operating at the low-force limits of the DMA in the range of 10 mN [64]. So, care should be taken when interpreting the absolute values of the rubbery modulus. The undercured specimens exhibit decreased network density $\nu_{e,m}$ calculated from the rubbery modulus (Table S3) and swelling experiments $\nu_{e,s}$ (Table S5) so that we expect a more flexible network with increased plasticity that can be beneficial for the malleability and processing of dynamic networks. The ratio $\nu_{e,m}/\nu_{e,s}$ (Figure S3) is particularly pronounced for the low network densities, indicating that the actual cure-dependent variation in network densities may be smaller than suggested by the tremendous change in rubbery modulus values. Considering the extrapolation of the characteristic temperature (T_v) according to the Maxwell relation for viscoelastic fluids with a relaxation time $\tau^* = \eta/G$, with G being the rubbery shear modulus and η the shear viscosity (10^{12} Pas [3]) at the liquid-to-glass transition,

underestimated rubbery moduli E'[1] would significantly reduce the extrapolated viscoelastic solid to the viscoelastic liquid transition temperature.

3.4 | Cure-Dependent Relaxation Behavior

Tensile stress relaxation trials of the fully cured state are conducted in a broad temperature range (100°C–220°C, Figure 2b). The lower boundary of 100°C was selected as the fully cured material remains a constant rubbery modulus above this temperature (cf. Figure 2a). We choose the Kohlrausch–Williams–Watts (KWW) stretched exponential decay [65] to fit the tensile stress relaxation response for the different cure-states separately (Figure S4):

$$\frac{E(t)}{E_0} = exp\left[-\left(\frac{t}{\tau^*}\right)^{\beta}\right], \tag{5}$$

where τ^* represents the relaxation time, β the stretching exponent, and $E(t)$ the decay in relaxation modulus at time t related to its initial value E_0. The β values ($0 < \beta \leq 1$) describe the width of the relaxation time distribution, with lower β values associated with greater width and more heterogeneous segmental dynamics [66]. The parameters β and τ^* are fitted for each temperature (Figure S4) and subsequently the average relaxation time is calculated as follows [67]:

$$\langle\tau\rangle = \frac{\tau^*\Gamma\left(\frac{1}{\beta}\right)}{\beta}, \tag{6}$$

where Γ is the gamma function. The activation energies E_a of flow is calculated assuming an Arrhenius-like behavior of the average relaxation time $\langle\tau\rangle = \tau_0 \exp\left(\frac{E_a}{RT}\right)$, with E_a being calculated to 109 kJ mol^{-1}, which is in the range of disulfide vitrimers reported in literature [5, 6, 68]. Even for the investigated broad temperature range, an excellent Arrhenius-type temperature dependence of relaxation times was obtained with R^2 located above 0.99 (Figure 2c). The stretching coefficient β values (Figure 2c, Table S6) range from 0.58 to 0.73 and are dependent on the temperature, proposing a gradual relaxation homogeneity increase with increasing temperature. At elevated temperatures, the disulfide bonds situated within flexible chain segments are less influenced by segmental motion and can exchange more freely, resulting in a more singular relaxation process [36]. At lower temperatures, the effects of the glass transition become noticeable, partly constraining the segmental motion and resulting in a less singular relaxation process. Therefore, a temperature of 140°C is selected to analyze the undercured states to minimize the effects of the glass transition and, simultaneously, to rule out significant advancement of the curing process relaxation tests.

Tensile stress relaxation trials of the partly cured states $T_{g,1}$–$T_{g,5}$ (Figure 2d) quantify the disulfide bond exchange kinetics and segmental relaxation at different cure states. Figure 3a shows the KWW fit of the normalized stress relaxation data at 140°C, and Figure 3b shows the apparent cure dependence of β and $\langle\tau\rangle$. Apparently, we observe a gradual increase of stretching with increasing cure state (β declining from ~0.83 to ~0.61), suggesting a gradual increase of relaxation heterogeneity with increasing cure-state. Generally assuming that glasses exhibit dynamical heterogeneities and that such heterogeneities disappear as the material is heated far above T_g [66], a greater $\Delta T_i = 140^{\circ}C - T_{g,i}$ facilitates a more homogeneous relaxation time distribution. Still, even ΔT values of ~130 K show a stretched relaxation and are not sufficient to homogenize the decay to a single exponential function ($\beta = 1$) and may be associated with the ongoing curing process (cf. Figure S5, Table S7) or the soluble fractions and accompanied network heterogeneities broadening the relaxation spectrum. The model predicts post-curing contributions of 0.02–0.04 during the initial dwelling period and an additional 0.02–0.04 during the measurement phase, resulting in both the ξ after soaking and the apparent ξ observed during testing located above the initial ξ_0 value. For evaluation in Figure 3b, the mean value of T_g calculated from the apparent ξ values observed during testing is employed to account for the advancing reaction.

In the undercure states, the average relaxation time $\langle\tau\rangle$ significantly decreases by a factor of ~30 (Figure 3b, Table S8), showcasing the superimposed effect of (i) increased segmental motion and S—S mobility due to reduced network density ν_e (cf. Tables S3 and S5)—a function of unreacted primary/secondary amines; and (ii) catalytic activity of unreacted amines on S—S exchange. These superimposed effects appear to be very effective in temporarily reducing relaxation times and offer the potential to be applied explicitly during processing to lower viscosity and potentially open up "melt" processing for vitrimers. Based on our investigations, we provide a statement regarding the cumulative effects of (i) and (ii), although it remains challenging to deconvolute individual contributions. The aliphatic monomer produces extended linear polymer strands between crosslinks, which generally results in longer relaxation times. Consequently, the dynamic exchange of disulfide bonds may not represent the sole rate-limiting mechanism. In contrast, intermediate cure states and associated lower crosslink densities significantly shorten relaxation times, thereby complicating the deconvolution of the individual contributions from segmental relaxation and bond exchange kinetics—even considering recent theoretical advances suggesting an intricate interconnection between these two processes [69, 70].

Indeed, reduced network densities can be reached by changing the stoichiometry of the amine-epoxy groups. Still, this yields deterioration of mechanical properties [71] and is not desirable. Therefore, utilizing partly cured states can guarantee sufficient mechanical properties in the final cured state and temporarily accelerate segmental relaxation and dynamic bond exchange rates. Besides the segmental relaxation and dynamic bond exchange rates, the following section focuses on the cure dependence of the onset of plastic flow characterized by the topology freezing temperature.

3.5 | Thermomechanical Analysis to Investigate Cure Dependence of the Vitrimer Transition Temperature

Thermomechanical analysis has proven a well-suited approach to detect malleability-induced shape changes of vitrimer

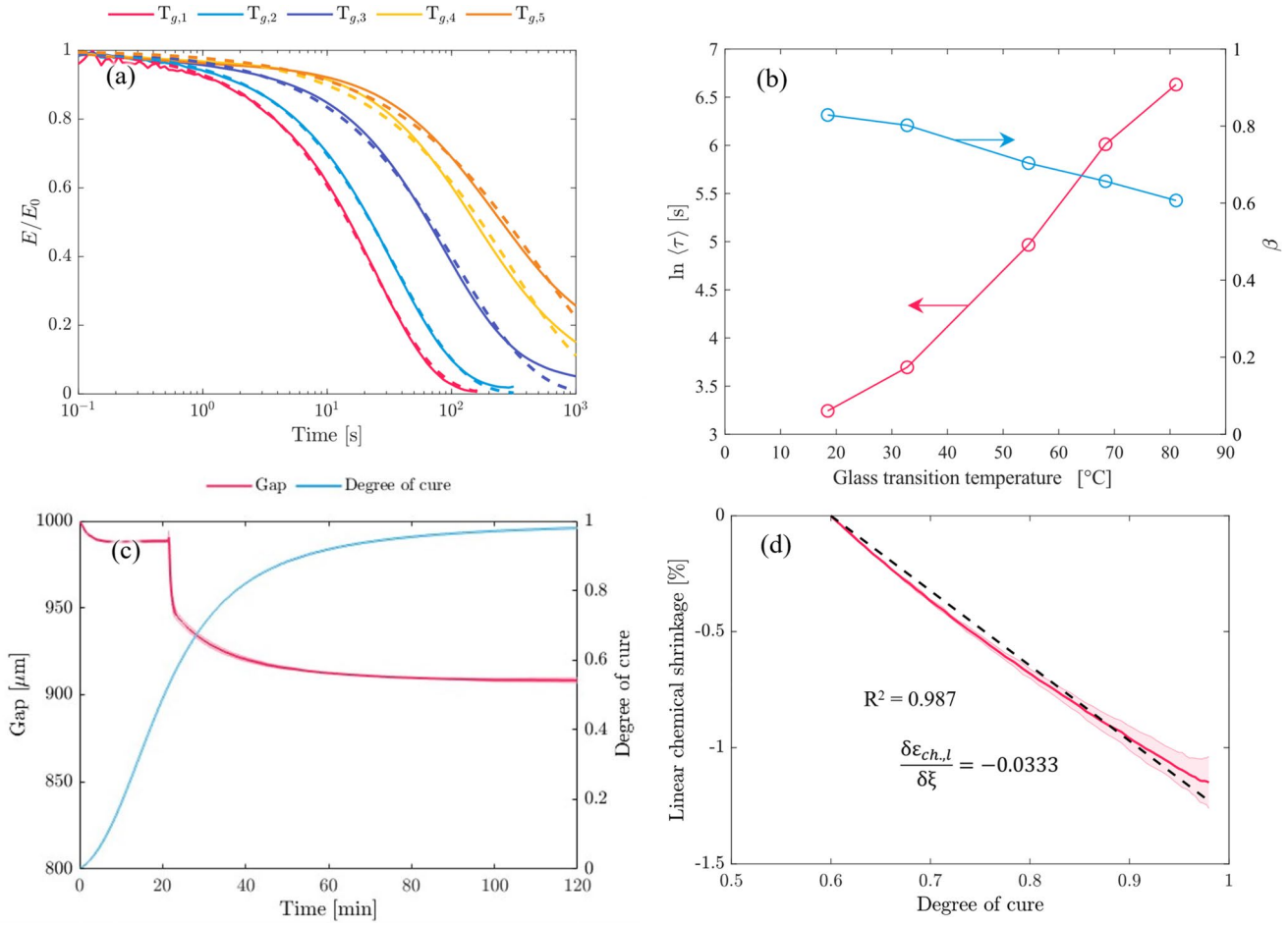

FIGURE 3 | Normalized stress-relaxation curves and dashed fit according to the Kohlrausch–Williams–Watts function (a). Cure dependence of stretching exponent β and average relaxation times $\langle\tau\rangle$ (b). The gap change was recorded during isothermal dwellings in the rheometer, and the curing process was calculated utilizing the recorded temperature profile (c). Cure dependence of chemical shrinkage strain (d).

materials [28, 29]. Still, unlike fully cured specimens, the total strain $\varepsilon_t = \varepsilon_{th} + \varepsilon_{ch}$ of partly cured specimens compromises a thermal ε_{th} and a chemical ε_{ch} contribution. The chemical contributions result from the chemical shrinkage (2–7 vol.-% for epoxy resins [72–75] corresponding to linear strain values ε_{ch} of 0.67%–2.28% [2]), causing a negative strain counteracting the thermal expansion during the heating ramp applied in the TMA. Therefore, it is crucial to quantify the negative strain to clearly identify the actual vertex of the solely temperature-dependent thermal strain to identify uniquely T_v. For this, we utilize the linear correlation of the chemical shrinkage and curing reaction, which has been demonstrated in numerous studies for epoxy resins [43, 72] and vitrimers [9]. We use a two-step protocol [43] to determine the linear chemical shrinkage strain occurring during the curing reaction (Figure S6). The cure-induced gap-change and the present temperature profile are recorded during the second, normal-force controlled isothermal dwelling step. Equations (1,2) are solved for the recorded temperature, enabling us to predict the curing degree during the isothermal dwelling step (Figure 3c), and the recorded gap change is transformed into the linear chemical shrinkage strain $\varepsilon_{ch.,l}$ described by Equations (S10, S11). Plotting the linear chemical shrinkage versus the degree of cure development yields a close-to-linear correlation (Figure 3d) with R^2 values of 0.987, stating a good correlation. These correlation facilitates the prediction of post-curing behavior and chemically induced strain during TMA heating, particularly in samples exhibiting intermediate cure states and elevated sol fractions indicative of residual unreacted monomers (Table S5).

Figure 4a shows the total superimposed (contributions of thermal expansion and chemical shrinkage) strain and the adjusted curves by adding the chemical strain contribution (dashed). Independently of the cure-state, the thermal strain derivative (Figure 4b) exhibits constant values of 68–71·10^{-6} K^{-1} (Figure S8, Table S9) and represents the coefficient of thermal expansions (CTE) in the glassy state. The values are located in the typical range of epoxy resins in the glassy state [72, 73, 77]. In the glassy state, the mobility of the molecules remains limited, so the effect of network formation on the expansion properties of the glass is of subordinate importance. Conversely, for $T > T_g$, mobility of the molecules increases. As a result of the higher molecular mobility, the advancing network structure (with increased cure-state) increasingly reduces the mobility of the molecules. Thus, a higher network density constraints the polymer chains and reduces mobility yielding smaller CTE values [73, 78]. Therefore, the thermal strain derivative shows a second plateau that describes the CTE in the rubbery state with values ranging

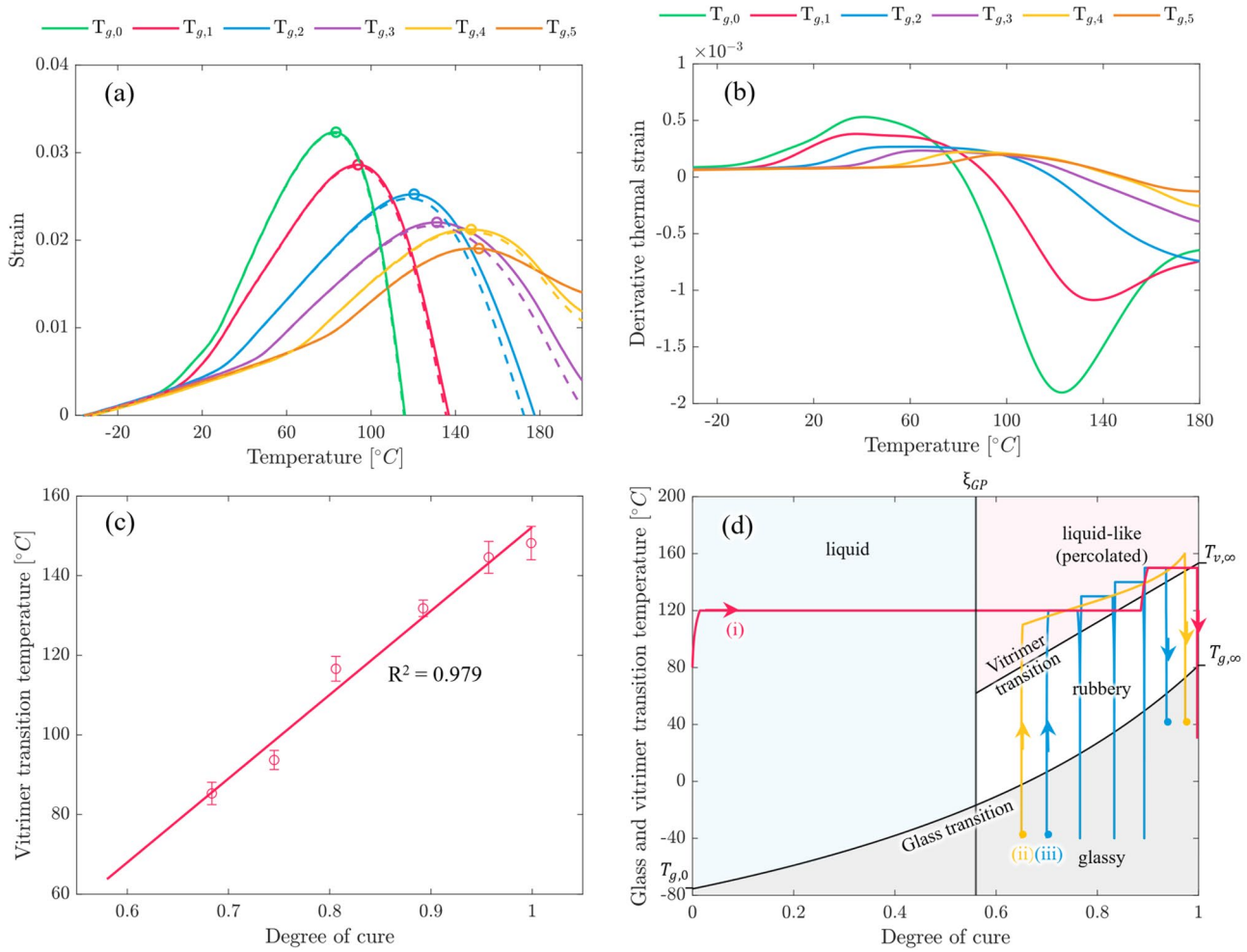

FIGURE 4 | Expansion strains were recorded during the thermomechanical analysis. The solid lines show the superimposed total strain, while the dashed lines show the curve adjusted by the chemical strain contribution. Maximum values to identify T_v are indicated (a). Derivative thermal strain curves extracted from the dashed curved in (a) implicitly identify glassy and rubbery regimes (b). Cure dependence of T_v approximated by a linear fit (c). Conversion–temperature phase diagram considering cure dependence of T_g and T_v while including generic processing cycles (i–iii) of partly cured materials (d).

from $194 \pm 5 \cdot 10^{-6}\,K^{-1}$ for the fully cured up to $495 \pm 30 \cdot 10^{-6}\,K^{-1}$ for $T_{g,0}$ (Figure S8, Table S9).

According to Hubbard et al., the peak value represents the vitrimer transition T_v and the presence of dynamic covalent bond exchange [29]. Therefore, the circles in Figure 4a identify the maximum values indicating T_v and are summarized in Table S9. Furthermore, it becomes apparent that the reaction process proceeds during the heating ramp, reporting small increases of 0.01–0.02 up to reaching T_v (Table S9). Still, in Figure 4c a strong cure dependence of T_v is observed, which shows a close-to-linear correlation with the apparent degree of cure at T_v (Table S9). The partly cured states shift the initiation of viscoelastic flow to lower temperature regimes, confirming the significantly decreased relaxation times, which already indicated an increased considerably bond exchange rate. Therefore, the bond exchange rates of disulfides significantly increase in the partially cured state and may be utilized to control relaxation times and viscosity to improve the manufacturing capabilities of the vitrimer system. To assess the broader implications of the reduced T_v in intermediate cure states and extract actionable insights for processing, the previous results are consolidated into a CTP diagram, which is discussed in the following section.

3.6 | Conversion–Temperature Phase Diagram

Processing a vitrimer is a rather complex process involving transitions and various partly superimposed transformations. This circumstance necessitates a distinct representation in a transformation diagram to understand the material behavior and facilitate thoughtful advanced process design. Conversion–temperature phase diagrams (CTP) constitute valuable tools for representing main transformations such as gelation, vitrification, and vitrimer transition during the processing of vitrimer resins and, therefore, are well suited to investigate different complex curing kinetic steps.

Compiling reaction kinetics, gelation measurements, cure-dependent glass, and vitrimer transition temperatures enables us

to construct a CTP diagram according to Adabbo and Williams [79], depicted in Figure 4d. Figure 4d indicates distinct phases: glassy, liquid, rubbery, and liquid-like and associated transitions. In our study, the key novelty is the introduction of a cure-dependent T_v, delineating the transition between viscoelastic rubber and viscoelastic fluid with macroscopic flow. Nonetheless, it is essential to note that T_v does not represent a sharp transition attributed to a distinct temperature. Instead, it exhibits a more gradual transition whose characteristics are influenced by external parameters such as mechanical loading [29, 30].

Various generic curing cycles (i–iii) (Table S10) are drawn to demonstrate exemplary application: For cycle (i), the resin first gels and transitions directly from the liquid into the liquid-like percolated region. With the reaction proceeding during the isothermal dwelling at 120°C, the resin undergoes liquid-to-rubber transition at $\xi \sim 0.82$. After subsequently increasing the temperature to 150°C, a percolated fluid is restored before the network reverts to the rubbery state until the end of the curing process.

Particularly interesting is the liquid-like percolated region, which is accompanied by fast dynamic bond exchange rates. So, designing manufacturing processes that utilize accelerated segmental relaxation and bond exchange is desirable. The cure cycle (ii, Table S10) illustrates a ramped heating that maintains the percolated fluid state for 80 min before cooling in the glassy state. It, therefore, seems plausible to utilize this timeframe for continuous processing (e.g., extrusion) and harvest the decreased viscosities elicited by the low crosslinking densities and accelerated segmental relaxation and bond exchange rates. Still, it is also essential to consider the proceeding curing reaction and the accompanying development of crosslinking density and mechanical modulus. Another scenario (iii, Table S10) involves designing a single discontinuous or multiple consecutive isothermal dwelling cycles (e.g., multistep thermoforming) to utilize the advanced malleability in the partially crosslinked state.

Therefore, the CTP diagram enables us to delineate processing cycles capable of sustaining the viscoelastic-plastic flow regime with enhanced dynamic covalent bond exchange kinetics for durations exceeding 60 min while concurrently suppressing the extent of cure advancement. This processing window facilitates reactive processing of the percolated network at reduced viscosities, which may be advantageous for shaping and consolidation operations. Nonetheless, these conditions must be contextualized within the framework of a specific processing protocol. Particular attention must be paid to boundary conditions, as secondary thermal contributions during processing—arising from internal frictional heating (e.g., shear heating in screw processing) or exothermic residual cure reactions—may induce significant deviations from the prescribed time–temperature trajectory.

4 | Conclusion

In conclusion, we have examined the cure-state dependence of disulfide bond exchange rates and T_v. Our primary interest was quantifying the effect of transient partly cured states on the associative bond exchange dynamics and accompanied viscosity to provide new perspectives for bridging the high-viscosity behavior of vitrimers with the processability requirements of conventional polymer manufacturing. Stress relaxation tests on partially cured specimens demonstrate that the relaxation times may be reduced by at least one magnitude and thus suggest that in the partially crosslinked state, the dynamic bond exchange and segmental relaxation rates are significantly accelerated, likely due to the lower crosslinking density and the catalytic effects from free pending amine groups. Therefore, further studies are required to deconvolute the contributions of segmental motion and bond exchange reactions in a selective manner.

Another aspect of this work was to explore the cure dependence of the dynamic nature of aromatic disulfide bonds within a transient network and if the dynamic bond exchange remains permissible for partly cured systems at mild temperatures. Therefore, we employ thermomechanical analysis to detect the transition of a transient network subjected to applied stress from entropy elastic to the plastic flow regime. A phenomenological approach allows us to separate the change in strain due to thermal expansion from that triggered by post-curing shrinkage. Thus, we can demonstrate an evident effect of the cure state on the onset of the plastic flow regime tied to the temperature T_v which may be associated with the presence of associative dynamic covalent bond exchange reactions. The key observation was that T_v linearly depends on the cure state and increases with increasing crosslinking density. Finally, we consolidate all data into a conversion–temperature phase diagram accounting for the cure dependence of T_v. For the investigated dynamic disulfide epoxy network, we identify a processing window that maintains the plastic flow regime with accelerated bond exchange rates for more than 1 h while minimizing the cure progress. This provides sufficient time for the reactive processing of the percolated fluid with reduced viscosity. However, practical implementation requires careful consideration of process-specific factors such as internal friction and residual reaction heat, which may cause deviations from the intended time–temperature cycle.

Although the reported relaxation times may not yet support true "melt" processing of vitrimers, we hope the results of this work will provide a foundation for tailoring disulfide-based vitrimer systems to specific processing needs and open new opportunities for engineering applications that leverage reactive processing in the partially cured state.

Acknowledgments

This project is made possible partly by a contribution from the National Growth Fund program NXTGEN HIGHTECH 01 (NGFNH2201). The authors acknowledge continuous support from the ASM department and technical staff.

Conflicts of Interest

The authors declare no conflicts of interest.

Data Availability Statement

The data that support the findings of this study are available from the corresponding author upon reasonable request.

Endnotes

[1] Assuming homogeneous isotropic behavior and Poisson's ratio ν of 0.5 in the rubbery state and utilizing Lamé coefficients, G may be substituted with $E^{'}/(2(1+\nu))$.

[2] $\varepsilon_{ch} = \left(1-\varepsilon_{ch,vol.}\right)^{1/3} - 1$, with $\varepsilon_{ch,vol.}$ corresponding to the volumetric change caused by chemical shrinkage [43, 76].

References

1. S. Maes, N. Badi, J. M. Winne, and F. E. Du Prez, "Taking Dynamic Covalent Chemistry Out of the Lab and Into Reprocessable Industrial Thermosets," *Nature Reviews Chemistry* 1 (2025): 1–15.

2. Y. Yang, Y. Xu, Y. Ji, and Y. Wei, "Functional Epoxy Vitrimers and Composites," *Progress in Materials Science* 120 (2021): 100710.

3. D. Montarnal, M. Capelot, F. Tournilhac, and L. Leibler, "Silica-Like Malleable Materials From Permanent Organic Networks," *Science* 334 (2011): 965–968.

4. B. Lewis, J. M. Dennis, C. Park, and K. R. Shull, "Glassy Dynamics of Epoxy-Amine Thermosets Containing Dynamic, Aromatic Disulfides," *Macromolecules* 57 (2024): 4c01012, https://doi.org/10.1021/acs.macromol.4c01012.

5. I. Azcune, E. Elorza, A. Ruiz De Luzuriaga, A. Huegun, A. Rekondo, and H.-J. Grande, "Analysis of the Effect of Network Structure and Disulfide Concentration on Vitrimer Properties," *Polymers* 15 (2023): 4123.

6. A. Ruiz de Luzuriaga, G. Solera, I. Azcarate-Ascasua, V. Boucher, H.-J. Grande, and A. Rekondo, "Chemical Control of the Aromatic Disulfide Exchange Kinetics for Tailor-Made Epoxy Vitrimers," *Polymer* 239 (2022): 124457.

7. N. Lorenz, W. E. Dyer, and B. Kumru, "High-Performance Vitrimer Entailing Renewable Plasticizer Engineered for Processability and Reactivity Toward Composite Applications," *ACS Applied Polymer Materials* 7 (2025): 1934.

8. J. Alms, A. K. Sambale, J. Fuchs, et al., "Qualification of the Vitrimeric Matrices in Industrial-Scale Wet Filament Winding Processes for Type-4 Pressure Vessels," *Polymers* 17 (2025): 1146.

9. N. Lorenz, T. Zawadzki, L. Keller, J. Fuchs, K. Fischer, and C. Hopmann, "Characterization and Modeling of an Epoxy Vitrimer Based on Disulfide Exchange for Wet Filament Winding Applications," *Polymer Engineering and Science* 64 (2024): 3682.

10. S. Zhao and M. M. Abu-Omar, "Recyclable and Malleable Epoxy Thermoset Bearing Aromatic Imine Bonds," *Macromolecules* 51 (2018): 9816–9824.

11. B. Li, G. Zhu, Y. Hao, and T. Ren, "Effect of Cross-Link Density on the Performance of Polyimine/Epoxy Vitrimers," *Smart Materials and Structures* 33 (2024): 025014.

12. N. Lorenz, W. E. Dyer, and B. Kumru, "Thermo-Rheological and Kinetic Characterization and Modeling of an Epoxy Vitrimer Based on Polyimine Exchange," *Soft Matter* 20 (2024): 6289–6301, https://doi.org/10.1039/D4SM00724G.

13. V. Amfilochiou, T. Debsharma, I. De Baere, L. Daelemans, F. Du Prez, and W. Van Paepegem, "Thermomechanical Characterisation of Reprocessable, Siloxane-Based, Glass-Fibre-Reinforced Vitrimersa," *Composites Part B: Engineering* 276 (2024): 111354.

14. T. Debsharma, V. Amfilochiou, A. A. Wróblewska, I. De Baere, W. Van Paepegem, and F. E. Du Prez, "Fast Dynamic Siloxane Exchange Mechanism for Reshapable Vitrimer Composites," *Journal of the American Chemical Society* 144 (2022): 12280–12289.

15. W. Denissen, G. Rivero, R. Nicolaÿ, L. Leibler, J. M. Winne, and F. E. Du Prez, "Vinylogous Urethane Vitrimers," *Advanced Functional Materials* 25 (2015): 2451–2457.

16. W. Alabiso and S. Schlögl, "The Impact of Vitrimers on the Industry of the Future: Chemistry, Properties and Sustainable Forward-Looking Applications," *Polymers* 12 (2020): 1660.

17. B. Krishnakumar, R. V. S. P. Sanka, W. H. Binder, V. Parthasarthy, S. Rana, and N. Karak, "Vitrimers: Associative Dynamic Covalent Adaptive Networks in Thermoset Polymers," *Chemical Engineering Journal* 385 (2020): 123820.

18. J. Studer, C. Dransfeld, and K. Masania, "An Analytical Model for B-Stage Joining and Co-Curing of Carbon Fibre Epoxy Composites," *Composites Part A: Applied Science and Manufacturing* 87 (2016): 282–289.

19. C. M. Yakacki, S. Willis, C. Luders, and K. Gall, "Deformation Limits in Shape-Memory Polymers," *Advanced Engineering Materials* 10 (2008): 112–119.

20. S. R. White, P. T. Mather, and M. J. Smith, "Characterization of the Cure-State of DGEBA-DDS Epoxy Using Ultrasonic, Dynamic Mechanical, and Thermal Probes," *Polymer Engineering and Science* 42 (2002): 51–67.

21. W. D. Cook, T. F. Scott, S. Quay-Thevenon, and J. S. Forsythe, "Dynamic Mechanical Thermal Analysis of Thermally Stable and Thermally Reactive Network Polymers," *Journal of Applied Polymer Science* 93 (2004): 1348–1359.

22. J. Gerritzen, M. Muller-Pabel, J. Muller, et al., "Development of a High-Fidelity Framework to Describe the Process-Dependent Viscoelasticity of a Fast-Curing Epoxy Matrix Resin Including Testing, Modelling, Calibration and Validation," *Polymers* 14 (2022): 3647.

23. M. J. Marks and R. V. Snelgrove, "Effect of Conversion on the Structure–Property Relationships of Amine-Cured Epoxy Thermosets," *ACS Applied Materials & Interfaces* 1 (2009): 921.

24. L. Sorrentino, W. Polini, and C. Bellini, "To Design the Cure Process of Thick Composite Parts: Experimental and Numerical Results," *Advanced Composite Materials* 23 (2014): 225–238.

25. B. Ellis, *Chemistry and Technology of Epoxy Resins* (Springer Netherlands, 1993).

26. J.-P. Pascault, H. Sautereau, J. Verdu, and R. J. J. Williams, *Thermosetting Polymers* (CRC Press, 2002), 519–533.

27. M. Capelot, M. M. Unterlass, F. Tournilhac, and L. Leibler, "Catalytic Control of the Vitrimer Glass Transition," *ACS Macro Letters* 1 (2012): 789–792.

28. A. Klingler, D. Reisinger, S. Schlögl, B. Wetzel, U. Breuer, and J.-K. Krüger, "Vitrimer Transition Phenomena From the Perspective of Thermal Volume Expansion and Shape (In)stability," *Macromolecules* 57 (2024): 4246–4253.

29. A. M. Hubbard, Y. Ren, A. Sarvestani, C. R. Picu, V. Varshney, and D. Nepal, "Thermomechanical Analysis (TMA) of Vitrimers," *Polymer Testing* 118 (2023): 107877.

30. S. Kaiser, P. Novak, M. Giebler, et al., "The Crucial Role of External Force in the Estimation of the Topology Freezing Transition Temperature of Vitrimers by Elongational Creep Measurements," *Polymer* 204 (2020): 122804.

31. H. Fang, W. Ye, Y. Ding, and H. H. Winter, "Rheology of the Critical Transition State of an Epoxy Vitrimer," *Macromolecules* 53 (2020): 4855–4862.

32. F. Meng, M. O. Saed, and E. M. Terentjev, "Rheology of Vitrimers," *Nature Communications* 13 (2022): 5753.

33. S. Weidmann, P. Volk, P. Mitschang, and N. Markaide, "Investigations on Thermoforming of Carbon Fiber Reinforced Epoxy Vitrimer Composites," *Composites Part A: Applied Science and Manufacturing* 154 (2022): 106791.

34. V. Amfilochiou, T. Debsharma, I. De Baere, L. Daelemans, F. Du Prez, and W. Van Paepegem, "Thermomechanical Characterisation of Reprocessable, Siloxane-Based, Glass-Fibre-Reinforced Vitrimers," *Composites Part B: Engineering* 276 (2024): 111354.

35. C. Taplan, M. Guerre, J. M. Winne, and F. E. D. Prez, "Fast Processing of Highly Crosslinked, Low-Viscosity Vitrimers," *Materials Horizons* 7 (2020): 104.

36. C. Wang, H. Xu, Z. Xie, J. Zheng, and J. Wu, "Extrudable, Robust and Recyclable Bio-Based Epoxy Vitrimer via Tailoring the Topology of a Dual Dynamic-Covalent-Bond Network," *Polymer* 289 (2023): 126487.

37. L. Farge, S. Hoppe, V. Daujat, F. Tournilhac, and S. André, "Solid Rheological Properties of PBT-Based Vitrimers," *Macromolecules* 54 (2021): 1838.

38. T. Isogai and M. Hayashi, "Seamless, Self-Transformation of Thermoplastic Polyesters Into Vitrimers Through Bond Exchange-Triggered Cross-Linking," *Macromolecular Rapid Communications* 45 (2024): 2400125.

39. J. J. Lessard, K. A. Stewart, and B. S. Sumerlin, "Controlling Dynamics of Associative Networks Through Primary Chain Length," *Macromolecules* 55 (2022): 10052–10061.

40. K. Yamawake and M. Hayashi, "The Role of Tertiary Amines as Internal Catalysts for Disulfide Exchange in Covalent Adaptable Networks," *Polymer Chemistry* 14 (2023): 680–686.

41. B. Li, G. Zhu, Y. Hao, and T. Ren, "An Investigation on the Performance of Epoxy Vitrimers Based on Disulfide Bond," *Journal of Applied Polymer Science* 139 (2022): 51589.

42. A. Rekondo, R. Martin, A. Ruiz De Luzuriaga, G. Cabañero, H. J. Grande, and I. Odriozola, "Catalyst-Free Room-Temperature Self-Healing Elastomers Based on Aromatic Disulfide Metathesis," *Materials Horizons* 1 (2014): 237–240.

43. M. Haider, P. Hubert, and L. Lessard, "Cure Shrinkage Characterization and Modeling of a Polyester Resin Containing Low Profile Additives," *Composites Part A: Applied Science and Manufacturing* 38 (2007): 994–1009.

44. V. Schenk, R. D'Elia, P. Olivier, K. Labastie, M. Destarac, and M. Guerre, "Exploring the Limits of High-*Tg* Epoxy Vitrimers Produced Through Resin-Transfer Molding," *ACS Applied Materials & Interfaces* 15 (2023): 46357.

45. A. Bernath, L. Karger, and F. Henning, "Accurate Cure Modeling for Isothermal Processing of Fast Curing Epoxy Resins," *Polymers* 8 (2016): 390.

46. D. Lahlali, M. Naffakh, and M. Dumon, "Cure Kinetics and Modeling of an Epoxy Resin Cross-Linked in the Presence of Two Different Diamine Hardeners," *Polymer Engineering & Science* 45 (2005): 1581–1589.

47. S. Sourour and M. R. Kamal, "Differential Scanning Calorimetry of Epoxy Cure: Isothermal Cure Kinetics," *Thermochimica Acta* 14 (1976): 41–59.

48. P. I. Karkanas, I. K. Partridge, and D. Attwood, "Modelling the Cure of a Commercial Epoxy Resin for Applications in Resin Transfer Moulding," *Polymer International* 41 (1996): 183–191.

49. P. I. Karkanas and I. K. Partridge, "Cure Modeling and Monitoring of Epoxy/Amine Resin Systems. I. Cure Kinetics Modeling," *Journal of Applied Polymer Science* 77 (2000): 1419–1431.

50. P. Navabpour, A. Nesbitt, B. Degamber, G. Fernando, T. Mann, and R. Day, "Comparison of the Curing Kinetics of the RTM6 Epoxy Resin System Using Differential Scanning Calorimetry and a Microwave-Heated Calorimeter," *Journal of Applied Polymer Science* 99 (2006): 3658–3668.

51. J.-P. Pascault and R. J. J. Williams, *Thermosets*, 2nd ed., ed. Q. Guo (Elsevier, 2018), 3.

52. J. P. Pascault and R. J. J. Williams, "Glass Transition Temperature Versus Conversion Relationships for Thermosetting Polymers," *Journal of Polymer Science Part B: Polymer Physics* 28 (1990): 85–95.

53. S. L. Simon and J. K. Gillham, "Thermosetting Cure Diagrams: Calculation and Application," *Journal of Applied Polymer Science* 53 (1994): 709–727.

54. S. Saseendran, M. Wysocki, and J. Varna, "Evolution of Viscoelastic Behavior of a Curing LY5052 Epoxy Resin in the Glassy State," *Advanced Manufacturing: Polymer & Composites Science* 2 (2016): 74–82.

55. C. M. Tung and P. J. Dynes, "Relationship Between Viscoelastic Properties and Gelation in Thermosetting Systems," *Journal of Applied Polymer Science* 27 (1982): 569.

56. F. Chambon and H. H. Winter, "Linear Viscoelasticity at the Gel Point of a Crosslinking PDMS With Imbalanced Stoichiometry," *Journal of Rheology* 31 (1987): 683–697.

57. R. Pethrick, "Real Time Dielectric Relaxation Studies of Dynamic Polymeric Systems," *Progress in Polymer Science* 27 (2002): 1983.

58. J. Farjas, J. A. González, D. Sánchez-Rodríguez, N. Blanco, M. Gascons, and J. Costa, "Analytical Criterion to Prevent Thermal Overshoot During Dynamic Curing of Thick Composite Laminates," *Advances in Industrial and Manufacturing Engineering* 10 (2025): 100156.

59. N. Lorenz, C. Hopmann, and K. Fischer, "Dielectric Monitoring of Gelation and Cure for Fast-Curing Epoxy Resins," *AIP Conference Proceedings* 3012 (2024): 020021.

60. N. Lorenz, R. Dahlmann, and C. Hopmann, *Experimentelle und Numerische Analyse der Oberflächenwelligkeit von Endlosfaserverstärkten Duroplastischen Faserverbundkunststoffen* (RWTH Aachen University, 2024).

61. T. S. Mesogitis, A. A. Skordos, and A. C. Long, "Uncertainty in the Manufacturing of Fibrous Thermosetting Composites: A Review," *Composites Part A: Applied Science and Manufacturing* 57 (2014): 67–75.

62. M. Müller, A. Winkler, M. Gude, and H. Jäger, "Aspects of Reproducibility and Stability for Partial Cure of Epoxy Matrix Resin," *Journal of Applied Polymer Science* 137 (2019): 48342.

63. A. R. Jagtap and A. More, "Developments in Reactive Diluents: A Review," *Polymer Bulletin* 79 (2022): 5667.

64. M. Müller-Pabel, J. A. Rodríguez Agudo, and M. Gude, "Measuring and Understanding Cure-Dependent Viscoelastic Properties of Epoxy Resin: A Review," *Polymer Testing* 114 (2022): 107701.

65. G. Williams and D. C. Watts, "Non-Symmetrical Dielectric Relaxation Behaviour Arising From a Simple Empirical Decay Function," *Transactions of the Faraday Society* 66 (1970): 80.

66. R. A. Riggleman, H.-N. Lee, M. D. Ediger, and J. J. de Pablo, "Heterogeneous Dynamics During Deformation of a Polymer Glass," *Soft Matter* 6 (2010): 287–291.

67. T. Wang, Y. Chen, B. Chen, M. J. Suazo, N. S. Purwanto, and J. M. Torkelson, "Reprocessable, Self-Healing, and Creep-Resistant Covalent Adaptable Network Made From Chain-Growth Monomers With Dynamic Covalent Thionourethane and Disulfide Cross-Links," *ACS Macro Letters* 13 (2024): 1147–1155.

68. R. Chen, L. Zhou, K. Zhang, and M. Chen, "Adjusting the Dynamic and Mechanochromic Properties of Aromatic Disulfide Epoxy Vitrimers by Unsaturation of Epoxy Monomers," *Journal of Applied Polymer Science* 141 (2024): e55655.

69. T.-W. Lin, B. Mei, S. Dutta, K. S. Schweizer, and C. E. Sing, "Molecular Dynamics Simulation and Theoretical Analysis of Structural Relaxation, Bond Exchange Dynamics, and Glass Transition in Vitrimers," *Macromolecules* 58 (2025): 1481–1497.

70. B. Mei, C. M. Evans, and K. S. Schweizer, "Self-Consistent Theory for Structural Relaxation, Dynamic Bond Exchange Times, and the Glass Transition in Polymeric Vitrimers," *Macromolecules* 57 (2024): 3242–3257.

71. H.-Y. Tsai, Y. Nakamura, W.-H. Hu, T. Fujita, and M. Naito, "Mechanochromism of Dynamic Disulfide Bonds as a Chromophoric Indicator of Adhesion Strength for Epoxy Adhesive," *Materials Advances* 2 (2021): 5047–5051.

72. N. Lorenz, M. Müller-Pabel, J. Gerritzen, et al., "Characterization and Modeling Cure- and Pressure-Dependent Thermo-Mechanical and Shrinkage Behavior of Fast Curing Epoxy Resins," *Polymer Testing* 108 (2022): 107498.

73. L. Khoun, T. Centea, and P. Hubert, "Characterization Methodology of Thermoset Resins for the Processing of Composite Materials — Case Study: CYCOM 890RTM Epoxy Resin," *Journal of Composite Materials* 44 (2009): 1397.

74. N. Lorenz, K. Fischer, and C. Hopmann, "Surface Waviness of Continuous Fiber-Reinforced Polymer Composites – a Review on Their Formation, Characterization and Modeling," *Composites Part A: Applied Science and Manufacturing* 198 (2025): 109067.

75. N. Lorenz, P. Hennes, K. Fischer, and C. Hopmann, "Surface Waviness of Continuous Fiber-Reinforced Thermosets–Experimental and Numerical Studies Considering the Viscoelasticity of the Resin," *Composites Part A: Applied Science and Manufacturing* 177 (2024): 107895.

76. J. Müller, M. Müller-Pabel, N. Lorenz, et al., "Visco-Thermo-Elastic Simulation Approach For Prediction of Cure-induced Residual Stresses in Fiber Reinforced Composites," https://popups.uliege.be/esaform21/index.php?id=4266.

77. M. Zarrelli, A. A. Skordos, and I. K. Partridge, "Investigation of Cure Induced Shrinkage in Unreinforced Epoxy Resin," *Plastics, Rubber and Composites* 31 (2013): 377.

78. A. Bandyopadhyay, P. K. Valavala, T. C. Clancy, K. E. Wise, and G. M. Odegard, "Molecular Modeling of Crosslinked Epoxy Polymers: The Effect of Crosslink Density on Thermomechanical Properties," *Polymer* 52 (2011): 2445–2452.

79. H. E. Adabbo and R. J. J. Williams, "The Evolution of Thermosetting Polymers in a Conversion–Temperature Phase Diagram," *Journal of Applied Polymer Science* 27 (1982): 1327–1334.

Supporting Information

Additional supporting information can be found online in the Supporting Information section.